EARTHQUAKE ENGINEERING AND STRUCTURAL DYNAMICS
Earthquake Engng Struct. Dyn. 2014; **00**:1–17
Published online in Wiley InterScience (www.interscience.wiley.com). DOI: 10.1002/eqe

arXiv:1403.5481v1 [stat.AP] 21 Mar 2014

Computing seismic fragility curves using non-parametric representations

B. Sudret [1], C.V. Mai [1], K. Konakli [1] *

[1] *ETH Zürich, Institute of Structural Engineering, Chair of Risk, Safety & Uncertainty Quantification, Stefano-Franscini-Platz 5, CH-8093 Zürich, Switzerland*

SUMMARY

Fragility curves are commonly used in civil engineering to estimate the vulnerability of structures to earthquakes. The probability of failure associated with a failure criterion (e.g. the maximal inter-storey drift ratio being greater than a prescribed threshold) is represented as a function of the intensity of the earthquake ground motion (e.g. peak ground acceleration or spectral acceleration). The classical approach consists in assuming a lognormal shape of the fragility curves. In this paper, we introduce two *non-parametric approaches* to establish the fragility curves without making any assumption, namely the conditional Monte Carlo simulation and the kernel density estimation. As an illustration, we compute the fragility curves of a 3-storey steel structure, accounting for the nonlinear behavior of the system. The curves obtained by the proposed approaches are compared with each other and with those obtained using the classical lognormal assumption. Copyright © 2014 John Wiley & Sons, Ltd.

Received . . .

KEY WORDS: earthquake engineering; fragility curves; lognormal assumption; non-parametric approach; kernel density estimation

1. INTRODUCTION

In recent years, *performance-based earthquake engineering* (PBEE) [1] (*seismic probabilistic risk assessment* (SPRA) [2] is the equivalent in the context of nuclear structural engineering) has arisen as a framework that supplements the usual deterministic design process. The latter aims at assuring primarily the performance of individual structural components, whereas PBEE allows one to address seismic performances at the system level and obtain probabilistic estimates of the risk of collapse and socio-economic impacts such as fatalities, repair costs, loss-of-use duration. A variety of performance objectives is incorporated into the design and analysis process using PBEE (or SPRA). This is of utmost importance due to the fact that a structure might not collapse during an earthquake, however, the cost for repairing, rebuilding or the downtime may not be acceptable [3]. The outcomes of PBEE are used by designers and owners as criteria in order to make better decisions in the design and management of structural systems.

In this probabilistic approach, *seismic fragility evaluation* is identified as one of the key elements together with hazard analysis and loss analysis. It consists in using *seismic fragility curves* to estimate the vulnerability of the considered structure (or its crucial components) to earthquakes, *i.e.* the probability that the structure (or the components) fails to fulfil a safety criterion during the ground motions. The probability of failure associated with a failure criterion (*e.g.* the maximal inter-storey drift ratio Δ being greater than a prescribed threshold δ_o) is represented as a function of

*Correspondence to: konakli@ibk.baug.ethz.ch

Copyright © 2014 John Wiley & Sons, Ltd.

the intensity of the earthquake motion (*e.g.* peak ground acceleration or spectral acceleration at the fundamental frequency [4]). From the mathematical point of view, a fragility curve represents the conditional probability that a prescribed threshold is attained or exceeded *given the intensity* of the ground motion.

First introduced in the early 1980's for nuclear safety evaluation [5], fragility curves are nowadays widely used for multiple purposes, *e.g.* seismic loss estimation [3], estimation of the collapse risk of structures in seismic regions [6], design checking process [7], evaluation of the effectiveness of retrofit measures [8], nuclear engineering [9], etc. One can classify fragility curves into four categories following the damage data sources, namely analytical, empirical, judgment-based or hybrid fragility curves [10]. Analytical fragility curves are derived from damage data obtained by analyses of structural models. Empirical fragility curves are based on the observation of earthquake-induced damage reported in post-earthquake surveys. Judgment-based curves are estimated by expert panels specialized in the field of earthquake engineering. Hybrid curves are typically obtained by combining data from different sources. Each category of fragility curves has its own advantages as well as drawbacks. In this paper, analytical fragility curves established using data collected from numerical structural analyses are of interest.

The classical approach to compute analytical fragility curves consists in assuming that the curves have the shape of a lognormal cumulative distribution function [11, 12]. This approach is therefore considered *parametric*. The parameters of the lognormal distribution are determined either by maximum likelihood estimation [11, 13, 14] or by fitting a linear probabilistic seismic demand model in the log-scale [15, 16, 17, 18].

For the purpose of validating the classical approach, we introduce two *non-parametric* approaches to establish the fragility curves *without* making any assumption, namely the Monte Carlo simulation (MCS) conditional on the intensity measure and the kernel density estimation (KDE).

The computation of fragility curves requires a large number of transient dynamic analysis of the structure under seismic excitations that are either recorded or synthetic. Due to the lack of recorded signals with the properties of interest (*e.g.* earthquake magnitude, duration, etc.), it is common practice to generate suitable samples of synthetic ground motions [19, 8]. This approach is used in the sequel.

The paper is organized as follows: in Section 2, the approach recently proposed by [20] to generate synthetic earthquakes, which are used in the example in Section 4, is briefly recalled. The different approaches for establishing the fragility curves, namely the classical lognormal, MCS-based and KDE-based approaches, are presented in Section 3. In Section 4 we compute the fragility curves of a steel frame structure subject to seismic excitations using the aforementioned approaches and compare the results.

2. RECORDED AND SYNTHETIC GROUND MOTIONS

2.1. *Recorded ground motions: notation*

Let us consider a recorded earthquake accelerogram $a(t)$, $t \in [0,T]$ where T is the total duration of the motion. The peak ground acceleration reads: $PGA = \max_{t\in[0,T]} |a(t)|$. The Arias intensity I_a is defined by:

$$I_a = \frac{\pi}{2g} \int_0^T a^2(t)\,\mathrm{d}t \tag{1}$$

Defining the cumulative square acceleration by:

$$I(t) = \frac{\pi}{2g} \int_0^t a^2(\tau)\,\mathrm{d}\tau\,, \tag{2}$$

one defines the time instant t_α by:

$$t_\alpha : \qquad I(t_\alpha) = \alpha I_a \qquad \alpha \in [0,1] \tag{3}$$

Copyright © 2014 John Wiley & Sons, Ltd.
Prepared using eqeauth.cls

DOI: 10.1002/eqe

Remarkable properties of a recorded seismic motion are the duration of the *strong motion phase* $D_{5-95} = t_{95\%} - t_{5\%}$ and the instant at the middle of the strong-shaking phase $t_{mid} \equiv t_{45\%}$.

2.2. *Simulation of synthetic ground motions*

In this section, we summarize the parameterized approach proposed by [20] in order to simulate synthetic ground motions. The seismic acceleration $a(t)$ is represented as a non-stationary process. Der Kiureghian and Rezaeian separate the non-stationarity into two components, namely a spectral and a temporal one, by means of a modulated filtered Gaussian white noise:

$$a(t) = \frac{q(t,\boldsymbol{\alpha})}{\sigma_h(t)} \int_0^t h\left[t-\tau, \boldsymbol{\lambda}(\tau)\right] \omega(\tau)\, \mathrm{d}\tau \tag{4}$$

in which $q(t,\boldsymbol{\alpha})$ is the deterministic non-negative *modulating function*, the integral is the non-stationary response of a linear filter subject to a Gaussian white noise excitation and $\sigma_h(t)$ is the standard deviation of the response process. The Gaussian white-noise process denoted by $\omega(\tau)$ will pass through a filter $h\left[t-\tau, \boldsymbol{\lambda}(\tau)\right]$ which is selected as the pseudo-acceleration response of a single-degree-of-freedom (SDOF) linear oscillator:

$$\begin{aligned} h\left[t-\tau, \boldsymbol{\lambda}(\tau)\right] &= 0 \quad \text{for} \quad t < \tau \\ h\left[t-\tau, \boldsymbol{\lambda}(\tau)\right] &= \frac{\omega_f(\tau)}{\sqrt{1-\zeta_f^2(\tau)}} \exp\left[-\zeta_f(\tau)\omega_f(\tau)(t-\tau)\right] \sin\left[\omega_f(\tau)\sqrt{1-\zeta_f^2(\tau)}(t-\tau)\right] \\ &\quad \text{for} \quad t \geq \tau \end{aligned} \tag{5}$$

where $\boldsymbol{\lambda}(\tau) = (\omega_f(\tau), \zeta_f(\tau))$ is the vector of time-varying parameters of the filter h. Note that $\omega_f(\tau)$ and $\zeta_f(\tau)$ are the filter's natural frequency and damping ratio at instant τ, respectively. They are related to the evolving predominant frequency and bandwidth of the ground motion that is to be represented. The statistical analysis of real signals shows that $\zeta_f(\tau)$ may be taken as a constant ($\zeta_f(\tau) \equiv \zeta$) while the predominant frequency varies approximately linearly in time [21]:

$$\omega_f(\tau) = \omega_{mid} + \omega'(\tau - t_{mid}) \tag{6}$$

In Eq. (6) t_{mid} is the instant at which 45% of the Arias intensity I_a is reached, $\omega_{mid} = \omega_f(t_{mid})$ is the filter's frequency at instant t_{mid} and ω' is the slope of the linear evolution. After being normalized by the standard deviation $\sigma_h(t)$, the integral in Eq. (4) becomes a unit variance process with time-varying frequency and constant bandwidth. The non-stationarity in intensity is then captured by the modulating function $q(t,\boldsymbol{\alpha})$. This time-modulating function determines the shape, intensity and duration T of the signal. A Gamma-like function is typically used [21]:

$$q(t,\boldsymbol{\alpha}) = \alpha_1 t^{\alpha_2 - 1} \exp(-\alpha_3 t) \tag{7}$$

where $\boldsymbol{\alpha} = \{\alpha_1, \alpha_2, \alpha_3\}$ is directly related to the energy content of the signal through the quantities I_a, D_{5-95} and t_{mid} defined in Section 2.1, see [21] for details. For computational purposes, the acceleration in Eq. (4) can be discretized as follows:

$$\hat{a}(t) = q(t,\boldsymbol{\alpha}) \sum_{i=1}^{n} s_i\left(t, \boldsymbol{\lambda}(t_i)\right) U_i \tag{8}$$

where the standard normal random variable U_i represents an impulse at instant $t_i = i \times \dfrac{T}{n}$, $i = 1, \ldots, n$, (T is the total duration) and $s_i(t, \boldsymbol{\lambda}(t_i))$ is given by:

$$s_i(t, \boldsymbol{\lambda}(t_i)) = \frac{h\left[t-t_i, \boldsymbol{\lambda}(t_i)\right]}{\sqrt{\sum_{j=1}^{i} h^2\left[t-t_j, \boldsymbol{\lambda}(t_j)\right]}} \tag{9}$$

Copyright © 2014 John Wiley & Sons, Ltd.
Prepared using eqeauth.cls

DOI: 10.1002/eqe

Note that the full model proposed by [21] includes some additional parameters that are related to earthquake and site characteristics, *e.g.* the type of faulting of the earthquake (strike-slip fault or reverse fault), the closest distance from the recording site to the ruptured area and the shear-wave velocity of the top 30 m of the site soil. For the sake of simplicity, these parameters are taken as deterministic in the sequel.

As a summary, the considered seismic generation model consists of three temporal parameters $(\alpha_1, \alpha_2, \alpha_3)$, three spectral parameters $(\omega_{mid}, \omega', \zeta_f)$ and the standard Gaussian random vector $\boldsymbol{U}$ of size n. As shown by [21], for a given recorded ground motion one can retrieve the values of these six parameters by fitting the energy and frequency content.

3. COMPUTATION OF FRAGILITY CURVES

Fragility curves represent the probability of failure of the system with respect to some performance criterion for a given intensity measure (IM) of the earthquake motion. The performance measure typically used for buildings is the so-called maximal inter-storey drift ratio Δ, *i.e.* the maximal difference of horizontal displacements between consecutive storeys normalized by the storey height [22]. Thus the fragility curve is cast as follows:

$$\text{Frag}(IM;\, \delta_o) = \mathbb{P}[\Delta \geq \delta_o | IM] \tag{10}$$

in which $\text{Frag}(IM;\, \delta_o)$ denotes the fragility at the given IM for a prescribed admissible threshold δ_o of the inter-storey drift ratio. In order to establish the fragility curves, a number N of transient finite element analyses of the structure under consideration are used to provide paired values $\{(IM_i, \Delta_i)\,, i = 1, \ldots, N\}$.

3.1. Classical approach

The classical approach to establish fragility curves consists in assuming a *lognormal shape* for the curves in Eq. (10). Two techniques are commonly used to estimate the parameters of the lognormal fragility curves, namely maximum likelihood estimation (MLE) and linear regression.

3.1.1. Maximum likelihood estimation: One assumes that the fragility curves can be written in the following general form:

$$\widehat{\text{Frag}}(IM;\, \delta_o) = \Phi\left(\frac{\log IM - \log \alpha}{\beta}\right) \tag{11}$$

where $\Phi\,(t) = \int_{-\infty}^{t} e^{-u^2/2}/\sqrt{2\pi}\mathrm{d}u$ is the standard Gaussian cumulative distribution function (CDF), α is the "median" and β is the "log-standard deviation" of the lognormal curve. We note that herein the terms median and log-standard deviation are merely used to describe the shape of the fragility curve and do not represent properties of a certain lognormally distributed random variable. The fragility curves are completely defined knowing α and β. [11] proposed the use of maximum likelihood estimation to determine these parameters as follows: Denote by ω the event that the damage corresponding to the prescribed threshold δ_o occurs. Assume that $Y(\omega)$ is a random variable with Bernoulli distribution, *i.e.* Y takes the value 1 (resp. 0) with probability $\text{Frag}(\cdot;\, \delta_o)$ (resp. $1 - \text{Frag}(\cdot;\, \delta_o)$). Considering a set of $i = 1, \ldots, N$ ground motions, the likelihood function reads:

$$\mathcal{L}\,(\alpha,\, \beta,\, \{IM_i,\, i = 1, \ldots, N\}) = \prod_{i=1}^{N} \left[\text{Frag}(IM_i;\, \delta_o)\right]^{y_i}\, \left[1 - \text{Frag}(IM_i;\, \delta_o)\right]^{1-y_i} \tag{12}$$

where IM_i is the intensity measure of the i^{th} seismic motion and y_i represents a realization of the Bernoulli random variable Y, which takes the value 1 or 0 depending on whether the structure under the i^{th} ground motion sustains the damage threshold δ_o or not. The parameters $(\alpha,\, \beta)$ are obtained by maximizing the likelihood function. In practice, a straightforward optimization algorithm is

Copyright © 2014 John Wiley & Sons, Ltd.
Prepared using eqeauth.cls

DOI: 10.1002/eqe

applied on the log-likelihood function, *i.e.* :

$$\{\alpha^*;\, \beta^*\}^{\mathsf{T}} = \arg\max \log \mathcal{L}\left(\alpha,\, \beta,\, \{IM_i,\, i = 1,\, \ldots\, , N\}\right) \tag{13}$$

3.1.2. Linear regression: One first assumes a *probabilistic seismic demand model* which relates a structural response quantity to an intensity measure of the earthquake motion. More specifically, the maximal inter-storey drift Δ is modelled by a lognormal distribution whose log-mean value is a *linear function* of $\log IM$:

$$\log \Delta = A\, \log IM + B + \zeta\, Z \tag{14}$$

where $Z \sim \mathcal{N}(0, 1)$ is a standard normal variable. Parameters A and B are determined by means of ordinary least squares estimation in a log-log plot. This approach is widely applied in the literature, see *e.g.* [19, 23, 24, 12] among others. The procedure is based on the assumed linear relationship between IM and Δ in the log-scale. Let us denote by e_i the residual between the actual value $\log \Delta$ and the value predicted by the linear model: $e_i = \log \Delta_i - A \log\left(IM_i\right) - B$. Parameter ζ is obtained by:

$$\zeta^2 = \sum_{i=1}^{N} e_i^2 / \left(N - 2\right) \tag{15}$$

Eq. (10) rewrites:

$$\begin{aligned} \widehat{\text{Frag}}(IM;\, \delta_o) &= \mathbb{P}\left[\log \Delta \geq \log \delta_o\right] = 1 - \mathbb{P}\left[\log \Delta \leq \log \delta_o\right] \\ &= \Phi\left(\frac{\log IM - \left(\log \delta_o - B\right)/A}{\zeta / A}\right) \end{aligned} \tag{16}$$

The median and log-standard deviation of the lognormal fragility curve in Eq. (16) are $\alpha = \exp\left[\left(\log \delta_o - B\right)/A\right]$ and $\beta = \zeta / A$ respectively.

The above so-called classical approach is *parametric* because it imposes the shape of the fragility curves in Eq. (11) and Eq. (16) which is similar to a lognormal CDF when considered as a function of IM. In the sequel, we propose two *non-parametric* approaches to compute fragility curves *without* making such an assumption.

3.2. Monte Carlo simulation approach

Having at hand a large sample set of pairs $\{\left(IM_j, \Delta_j\right),\, j = 1,\, \ldots\, , N\}$, it is possible to use *Monte Carlo simulation* (MCS) to compute the fragility curves. Let us consider a given abscissa IM_o. Within a small bin surrounding IM_o, say $[IM_o - h, IM_o + h]$ (see Figure 1) one assumes that the maximal drift Δ is linearly related to the IM. Note that this assumption is exact in the case of linear structures but would only be an approximation in the nonlinear case. Therefore, the maximal drift Δ_j related to $IM_j \in [IM_o - h, IM_o + h]$ is converted into the drift $\Delta_j(IM_o)$ which is related to a similar input signal having an intensity measure of IM_o as follows:

$$\Delta_j(IM_o) = \Delta_j \frac{IM_o}{IM_j} \tag{17}$$

The fragility curve at IM_o is obtained by a crude Monte Carlo estimator:

$$\widehat{\text{Frag}}(IM_o) = \frac{N_f\left(IM_o\right)}{N_s\left(IM_o\right)} \tag{18}$$

where $N_f\left(IM_o\right)$ is the number of points in the bin such that $\Delta_j(IM_o) \geqslant \delta_o$ and $N_s(IM_o)$ is the total number of points that fall into the bin $[IM_o - h, IM_o + h]$.

This MCS approach is similar to the incremental dynamic analysis (IDA) in [25] except that when using IDA, one scales *all* the ground motions to the intensity level of interest. Therefore in the IDA approach there are signals scaled with very large (or very small) scale factors compared to unity. The scaling procedure may induce a bias in the response of the structure [26, 27]. Figure 2 shows

Copyright © 2014 John Wiley & Sons, Ltd.

Prepared using eqeauth.cls
DOI: 10.1002/eqe

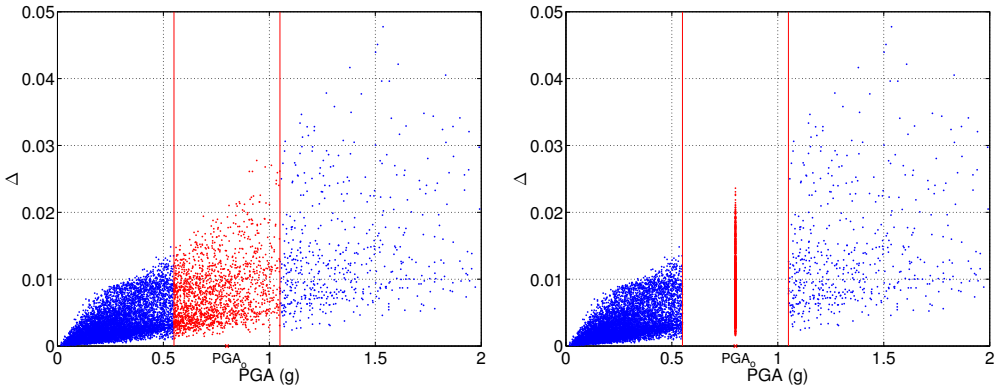

Figure 1. Scaling of ground motions and corresponding responses in the Monte Carlo simulation approach (the bin is enlarged for the sake of clarity).

the bias ratios induced by the scaling of ground motions for two different intensity measures. The bias for a certain scale factor is represented by the ratio of the mean maximal displacement response of a nonlinear SDOF system subject to the scaled motions to the respective response of the system without scaling of the motions. Note that the bias ratio becomes larger with increasing deviation of the scale factor from unity. In our approach, Eq. (17) basically represents the scaling of the ground motions in the vicinity of the intensity level IM_o. The vicinity is defined by the bin width $2h$ which is chosen so that the scale factors are close to 1. Accordingly, the bias due to ground motion scaling is negligible.

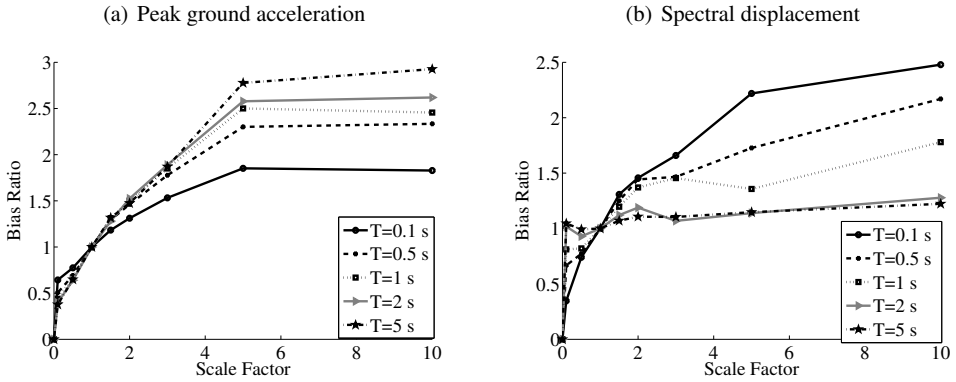

Figure 2. Bias ratios induced by the scaling of ground motions for two different intensity measures, namely peak ground acceleration and spectral displacement (after [26]).

3.3. Kernel density estimation

The fragility curves defined in Eq. (10) may be reformulated using the conditional probability density function (PDF) $f_{\Delta|IM}$ as follows:

$$\text{Frag}(a;\, \delta_o) = \mathbb{P}\left(\Delta \geq \delta_o | IM = a\right) = \int_{\delta_o}^{+\infty} f_{\Delta}(\delta | IM = a)\, \mathrm{d}\delta \tag{19}$$

Copyright © 2014 John Wiley & Sons, Ltd.
Prepared using eqeauth.cls

DOI: 10.1002/eqe

By definition this conditional PDF is given as:

$$f_{\Delta}(\delta|IM=a)=\frac{f_{\Delta,IM}(\delta,a)}{f_{IM}(a)} \tag{20}$$

where $f_{\Delta,IM}(\cdot)$ (resp. $f_{IM}(\cdot)$) is the joint distribution of the vector $(\Delta,\ IM)$ (resp. the marginal distribution of IM). If these quantities were known, the fragility curve in Eq. (19) would be obtained by a mere integration.

In this section we propose to *estimate* the joint and marginal PDFs from a sample set $\{(IM_i,\Delta_i),\ i=1,\ \ldots,N\}$ by *kernel density estimation* (KDE). For a single random variable X for which a sample set $\{x_1,\ \ldots,x_N\}$ is available, the kernel density estimate of the PDF reads [28]:

$$\hat{f}_X\left(x\right)=\frac{1}{Nh}\sum_{i=1}^{N}K\left(\frac{x-x_i}{h}\right) \tag{21}$$

where h is the *bandwidth* parameter and $K(\cdot)$ is the *kernel* function which integrates to one. Classical kernel functions are the Epanechnikov, uniform, normal and triangular functions. The choice of the kernel is known not to affect strongly the quality of the estimate [28] provided the sample set is large enough. In case a standard normal PDF is adopted for the kernel, *i.e.* $K(x)=\varphi(x)\equiv\exp\left[-x^2/2\right]/\sqrt{2\pi}$, the kernel density estimate rewrites:

$$\hat{f}_X\left(x\right)=\frac{1}{Nh}\sum_{i=1}^{N}\varphi\left(\frac{x-x_i}{h}\right) \tag{22}$$

In contrast, the choice of the bandwidth h is crucial for the kernel density estimate [29]. An inappropriate value of h can lead to an oversmoothed or undersmoothed estimated PDF. Eq. (22) is used for estimating the marginal distribution of the IMs, namely $\hat{f}_{IM}(a)$ from the set of intensity measures at hand, namely $\{IM_i,\ i=1,\ \ldots,N\}$:

$$\hat{f}_{IM}(a)=\frac{1}{Nh_{IM}}\sum_{i=1}^{N}\varphi\left(\frac{a-IM_i}{h_{IM}}\right) \tag{23}$$

Kernel density estimation may be extended to a random vector $\boldsymbol{X}\in\mathbb{R}^d$ given an i.i.d sample $\{\boldsymbol{x}_1,\ \ldots,\boldsymbol{x}_N\}$ [28]:

$$\hat{f}_{\boldsymbol{X}}\left(\boldsymbol{x}\right)=\frac{1}{N\left|\boldsymbol{H}\right|^{1/2}}\sum_{i=1}^{N}K\left(\boldsymbol{H}^{-1/2}(\boldsymbol{x}-\boldsymbol{x}_i)\right) \tag{24}$$

in which $\boldsymbol{H}$ is a symmetric positive definite *bandwidth matrix* whose determinant is denoted by $|\boldsymbol{H}|$. When a multivariate standard normal kernel is adopted, the joint distribution estimate becomes:

$$\hat{f}_{\boldsymbol{X}}\left(\boldsymbol{x}\right)=\frac{1}{N\left|\boldsymbol{H}\right|^{1/2}}\sum_{i=1}^{N}\frac{1}{\left(2\pi\right)^{d/2}}\exp\left[-\frac{1}{2}(\boldsymbol{x}-\boldsymbol{x}_i)^{\mathsf{T}}\boldsymbol{H}^{-1}(\boldsymbol{x}-\boldsymbol{x}_i)\right] \tag{25}$$

where $(\cdot)^{\mathsf{T}}$ denotes the transposition. For multivariate problems (*i.e.* $\boldsymbol{X}\in\mathbb{R}^d$), the bandwidth matrix classically belongs to one of the following classes: spherical, ellipsoidal and full matrix which contains respectively 1, d and $d(d+1)/2$ independent unknown parameters. This matrix $\boldsymbol{H}$ can be computed by means of *e.g.* plug-in and cross-validation estimators (see [29] for details). In the most general case when the correlations between the random variables are not known, the full matrix should be used. In this case, the *smoothed cross-validation estimator* is the most reliable among the cross-validation methods [30]. Using Eq. (25) to estimate the joint PDF $\hat{f}_{\Delta,IM}(\delta,a)$ from the data set $\{(IM_i,\ \Delta_i),\ i=1,\ \ldots,N\}$ one gets:

$$\hat{f}_{\Delta,IM}(\delta,a)=\frac{1}{2\pi N\left|\boldsymbol{H}\right|^{1/2}}\sum_{i=1}^{N}\exp\left[-\frac{1}{2}\begin{pmatrix}\delta-\Delta_i\\ a-IM_i\end{pmatrix}^{\mathsf{T}}\boldsymbol{H}^{-1}\begin{pmatrix}\delta-\Delta_i\\ a-IM_i\end{pmatrix}\right] \tag{26}$$

Copyright © 2014 John Wiley & Sons, Ltd.
Prepared using eqeauth.cls

DOI: 10.1002/eqe

The conditional PDF $f_\Delta(\delta|IM=a)$ is eventually estimated by pluging the estimations of the numerator and denominator in Eq. (20). The proposed estimator of the fragility curve eventually reads:

$$\widehat{\text{Frag}}(a;\,\delta_o) = \frac{h_{IM}}{2\pi\,|\boldsymbol{H}|^{1/2}} \frac{\displaystyle\int_{\delta_o}^{+\infty} \sum_{i=1}^{N} \exp\left[-\frac{1}{2}\begin{pmatrix}\delta-\Delta_i\\ a-IM_i\end{pmatrix}^{\mathsf{T}} \boldsymbol{H}^{-1} \begin{pmatrix}\delta-\Delta_i\\ a-IM_i\end{pmatrix}\right] \mathrm{d}\delta}{\displaystyle\sum_{i=1}^{N} \varphi\left(\frac{a-IM_i}{h_{IM}}\right)} \tag{27}$$

The choice of the bandwidth parameter h and the bandwidth matrix $\boldsymbol{H}$ plays a crucial role in the estimation of fragility curves, as seen in Eq. (27). In the above formulation, the same bandwidth is considered for the whole range of the IM values. However, there are typically few observations corresponding to the upper tail of the distribution of IM. This is due to the fact that the annual frequency of seismic motions with IM values in the respective range (*e.g.* PGA exceeding $1g$) is low (see *e.g.* [31]). This is also the case when synthetic ground motions are used, since these are generated consistently with the statistical features of recorded motions. Preliminary investigations have shown that by applying the KDE method on the data in the original scale, the fragility curves for the higher levels of damage tend to be unstable in their upper tails [32]. To reduce effects of the scarcity of observations at large IM values, we propose the use of KDE in the logarithmic scale, as described next.

Let us consider two random variables X, Y with positive supports and their logarithmic transformations $U=\log X$ and $V=\log Y$. The probability contained in a differential area must be invariant under the change of variables. In the one-dimensional case, this leads to:

$$f_X(x) = \left|\frac{\mathrm{d}u}{\mathrm{d}x}\right| f_U(U) = \left|\frac{1}{x}\right| f_U(u) = \frac{1}{x} f_U(u) \tag{28}$$

In the two-dimensional case, one obtains:

$$f_{X,Y}(x,y) = \frac{1}{x\,y} f_{U,V}(u,v) \tag{29}$$

Using Equations (28) and (29), one has:

$$\int_{y_0}^{+\infty} f_Y(y|X=x)\,\mathrm{d}y = \int_{y_0}^{+\infty} \frac{f_{X,Y}(x,y)}{f_X(x)}\,\mathrm{d}y = \int_{\log y_0}^{+\infty} \frac{\frac{1}{x\,y} f_{U,V}(u,v)}{\frac{1}{x} f_U(u)}\,y\,\mathrm{d}v = \int_{\log y_0}^{+\infty} f_V(v|U=u)\,\mathrm{d}v \tag{30}$$

Accordingly, by considering $X=IM$ and $Y=\Delta$, the fragility curves defined in Eq. (19) can be estimated in terms of $U=\log IM$ and $V=\log\Delta$ as:

$$\widehat{\text{Frag}}(a;\,\delta_o) = \int_{\delta_o}^{+\infty} \hat{f}_\Delta(\delta|IM=a)\,\mathrm{d}\delta = \int_{\log\delta_o}^{+\infty} \hat{f}_V(v|U=\log a)\,\mathrm{d}v \tag{31}$$

Note that use of a constant bandwidth in the logarithmic scale is equivalent to the use of a varying bandwidth in the original scale, with larger bandwidths corresponding to larger values of IM. The resulting fragility curves are smoother than those obtained by applying KDE with the data in the original scale.

3.4. Statistical analysis of fragility curves

It is of importance in fragility analysis to investigate the uncertainty in the estimated curves. The theoretical approach to determine the variability of an estimator relies on repeating the estimation with an ensemble of different random samples. However, this approach is not feasible in

Copyright © 2014 John Wiley & Sons, Ltd.
Prepared using eqeauth.cls

DOI: 10.1002/eqe

earthquake engineering because the physical phenomena under consideration are not reproducible or because the high computational cost allows only a limited number of simulations. In this context, the *bootstrap resampling* technique [33] is deemed appropriate. Given a set of observations $\boldsymbol{X} = (X_1, \ldots, X_n)$ from an unspecified probability distribution F, the bootstrap method allows estimation of the statistics of a random variable that depends on both $\boldsymbol{X}$ and F in terms of the observed data $\boldsymbol{X}$ and their empirical distribution.

To estimate statistics of the fragility curves with the bootstrap method, we first draw M independent random samples *with replacement* from the original data set $\{(IM_i, \Delta_i), i = 1, \ldots, N\}$. These represent the so-called bootstrap samples. Each bootstrap sample has the same size N as the original sample, but the observations are different: in a particular sample, some of the original observations may appear multiple times while others may be missing. Next, we compute the fragility curves for each bootstrap sample using the approaches in Sections 3.1, 3.2 and 3.3. Finally, we perform statistical analysis of the so-obtained M bootstrap curves. In the subsequent example illustration, the above procedure is employed to evaluate the median and 95% confidence intervals of the estimated fragility curves.

In the following, the proposed non-parametric approaches, namely crude MCS and KDE, as well as the classical lognormal approach for estimation of fragility curves are demonstrated in an example application on a frame structure. The uncertainty in the estimation of the MCS- and KDE-based curves is also investigated.

4. ILLUSTRATION: STEEL FRAME STRUCTURE

4.1. Problem statement: 3-storey 3-span steel frame

We evaluate the fragility curves of a 3-storey 3-span steel frame structure with the following dimensions: storey-height $H = 3$ m, span-length $L = 5$ m (see Figure 3). The steel material has nonlinear isotropic hardening behavior following the uniaxial Giuffre-Menegotto-Pinto steel model as implemented in the finite element software OpenSees [34]. The Young's modulus of steel is equal to $E_0 = 205,000$ MPa, the yield strength is $f_y = 235$ MPa and the strain hardening ratio (ratio of the post-yield tangent to the initial value) is $b = 0.01$. Figure 3 depicts the hysteretic behavior of the steel material at a section of the frame for an example ground motion. The structural components are modelled with nonlinear elements with distributed plasticity along their lengths. The use of fiber sections allows modelling the plasticity over the element cross-sections [35]. The vertical load consists of dead-load (from the frame elements as well as the supported floors), and live load in accordance with Eurocode 1 [36] which result in a total distributed load on the beams $q = 20$ kN/m. The preliminary design is performed using the vertical loads to provide the necessary sections of columns and beams. The standard European I beams with designation IPE 300 R and IPE 330 R are chosen respectively for beams and columns. The dimensions of the sections are depicted in Figure 4. The first two natural periods (resp. frequencies) of the building obtained by modal analysis of the corresponding linear model are $T_1 = 0.42$ s and $T_2 = 0.13$ s (resp. $f_1 = 2.38$ Hz and $f_2 = 8.33$ Hz).

The structure is subject to ground motions represented by the acceleration time histories at the ground level. Each ground motion is modelled by 6 randomized parameters $(\alpha_1, \alpha_2, \alpha_3, \omega_{mid}, \omega', \zeta_f)$ directly related to the parameters in Table I and a Gaussian input vector $\boldsymbol{U}$ (Eq. (8)). Note that in order to obtain a sufficiently wide range of IM, we adopted the statistics of I_a, D_{5-95} and t_{mid} presented in [21]. The duration of each synthetic earthquake is computed based on the corresponding set of parameters $(\alpha_1, \alpha_2, \alpha_3)$ and is used to determine the size of the Gaussian vector $\boldsymbol{U}$. A set of four different synthetic ground motions is shown in Figure 5 for the sake of illustration. The finite element code OpenSees [34] is used to carry out transient dynamic analyses of the frame for a total of $N = 10^4$ synthetic ground motions.

Numerous IMs can be used to represent the earthquake severity, see *e.g.* [37]. Peak ground acceleration (PGA) is a convenient measure that is straightforward to obtain for a given ground motion and has been traditionally used in attenuation relationships and design codes. However, structural responses may exhibit large dispersions with respect to PGA, since they are also highly

Copyright © 2014 John Wiley & Sons, Ltd.
Prepared using eqeauth.cls

DOI: 10.1002/eqe

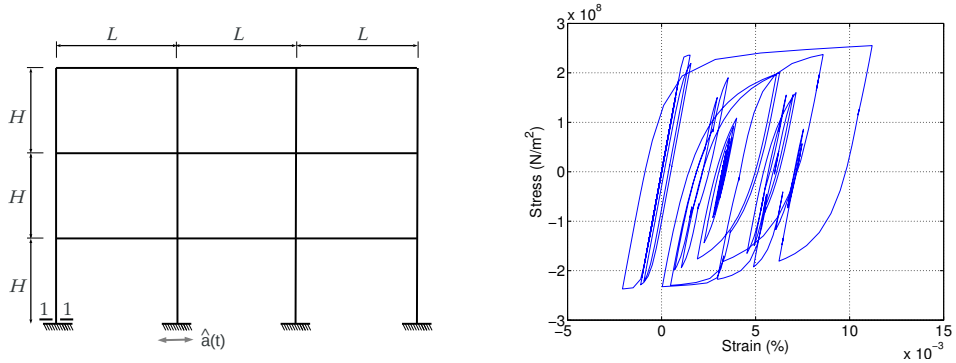

Figure 3. (Left) Steel frame structure. (Right) Hysteretic behavior of steel material at section 1-1 when the frame is subject to a particular ground motion.

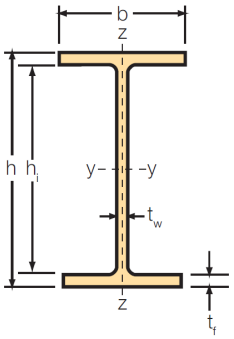

Figure 4. Cross-sections of beams (h=306 mm, b=147 mm, t_w=8,5 mm, t_f=13,7 mm) and columns (h = 336 mm, b=158 mm, t_w=9,2 mm, t_f=14,5 mm).

dependent on other features of earthquake motions, e.g. the frequency content and the duration of the strong motion phase. Structure-specific IMs, such as the spectral acceleration Sa, tend to be better correlated with structural responses [37, 38]. In the following, we compute fragility curves considering both PGA and Sa as IMs. In the present example, Sa represents $Sa(T_1)$ *i.e.* the spectral acceleration for a SDOF system with period equal to the fundamental period T_1 of the frame.

For each of the considered IMs, the pairs $\{(IM_i, \Delta_i), i = 1, \ldots, N\}$ are collected and post-processed following the approaches presented in Section 3 to establish the fragility curves for three drift thresholds, i.e. 0.7%, 1.5% and 2.5%. The drift thresholds 0.7% and 2.5% are recommended by [39] to respectively characterize light damage ("immediate occupancy" performance level) and moderate damage ("life safety" performance level) for steel frames. The drift threshold 1.5% corresponds to the damage limitation requirement for buildings with ductile non-structural elements according to [40].

4.2. Results

As described in Section 3, the lognormal approach consists in assuming that the fragility curves have the shape of a lognormal CDF and then estimating the parameters of the distribution. Using the MLE approach, the observed failures for each drift threshold are modeled as outcomes of a Bernoulli experiment and the parameters of the fragility curves are determined by maximizing the respective likelihood function. Using the linear regression technique, the parameters of the lognormal curves are indirectly derived by fitting a linear model to the paired data $(\log IM, \log \Delta)$. Figure 6 (resp. Figure 7) depicts the paired data $(\log PGA, \log \Delta)$ (resp. $(\log Sa, \log \Delta)$) and the fitted PSDM using linear regression. The coefficient of determination R^2 of the linear regression

Copyright © 2014 John Wiley & Sons, Ltd.
Prepared using eqeauth.cls

DOI: 10.1002/eqe

Table I. Statistics of parameters used to generate the synthetic ground motions (adapted from [21]).

Parameter	Distribution	Support	μ_X	σ_X
I_a	Lognormal	$(0, +\infty)$	5.613	10.486
D_{5-95}	Beta	[5, 20]	10	2
t_{mid}	Beta	[5, 15]	12	2
ω_{mid} / 2π	Gamma	$(0, +\infty)$	5.930	3.180
ω' / 2π	Two-sided exponential	[-2, 0.5]	-0.089	0.185
ζ_f	Beta	[0.02, 1]	0.210	0.150

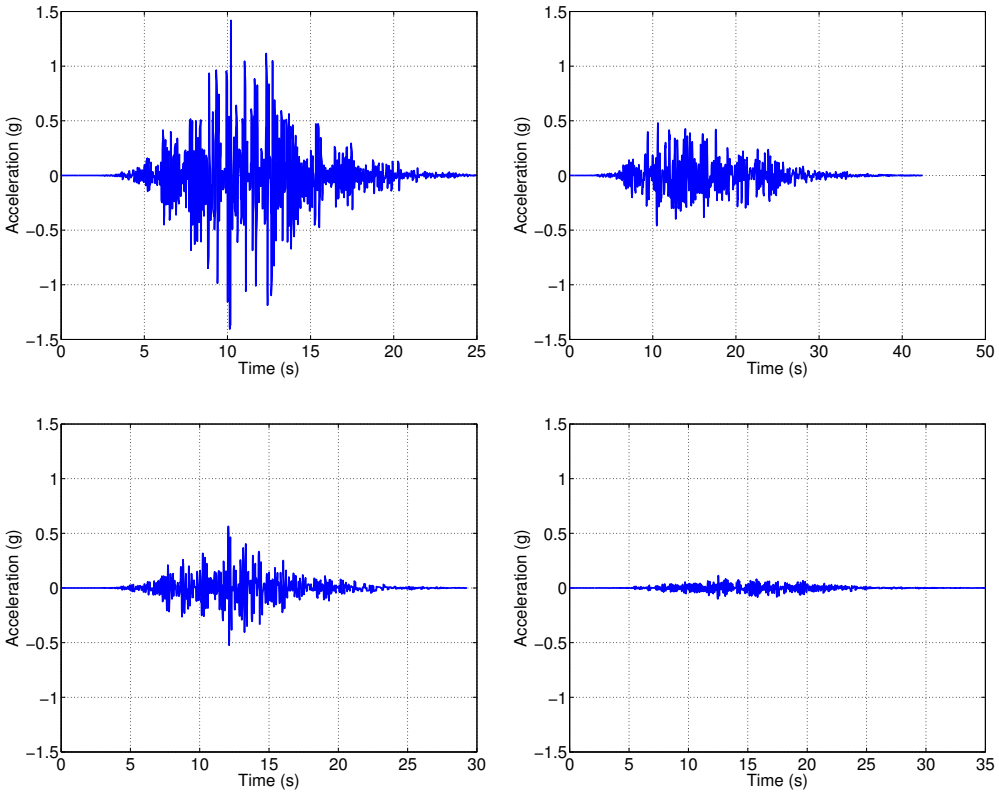

Figure 5. Examples of generated synthetic ground motions.

model considering PGA (resp. Sa) as an intensity measure is 0.603 (resp. 0.978). We observe that using Sa as an intensity measure leads to smaller dispersion *i.e.* smaller ζ in eqrefeeq8 as compared to using PGA. This is expected since Sa is a structure-specific IM. In the MCS method, the bandwidth h is set equal to $0.2\,IM_o$. The resulting scale factors vary in the range $[0.8,\ 1.2]$ yielding a bias ratio of approximately 1 (see Figure 2). Finally, the KDE approach requires estimation of the bandwidth parameter and the bandwidth matrix. Using the smoothed cross-validation estimation implemented in `R` [41], these are determined as $h = 0.1296$ and $\boldsymbol{H} = \begin{bmatrix} 0.0297 & 0.0240 \\ 0.0240 & 0.0279 \end{bmatrix}$ (resp. $h = 0.1778$ and $\boldsymbol{H} = \begin{bmatrix} 0.0144 & 0.0149 \\ 0.0149 & 0.0155 \end{bmatrix}$) when PGA (resp. Sa) is considered as IM.

For the two considered IMs and the three drift limits of interest, Table II lists the medians and log-standard deviations of the lognormal curves obtained with both the MLE and linear regression (LR) approaches. The median determines the position where the curve attains the value 0.5, whereas

Copyright © 2014 John Wiley & Sons, Ltd.
Prepared using eqeauth.cls

DOI: 10.1002/eqe

the log-standard deviation is a measure of the steepness of the curve. The medians of the KDE-based curves have been computed and are also listed in Table II for comparison. Using the KDE-based values as reference, one observes that in most cases MLE provides superior estimates of the medians as compared to linear regression. Note that the MLE approach yields a distinct log-standard deviation for each drift threshold, whereas a single log-standard deviation for all drift thresholds is obtained with the linear regression approach. The standard deviations obtained with MLE tend to be smaller than those obtained with linear regression in the case of PGA, but the reverse is true in the case of Sa.

Table II. Steel frame structure - Parameters of the obtained fragility curves.

		PGA		Sa	
δ_o	Approach	Median	Log-standard deviation	Median	Log-standard deviation
0.7%	MLE	$0.682\,g$	0.6338	$0.9630\,g$	0.2915
	LR	$0.7358\,g$	0.6229	$0.9869\,g$	0.1604
	KDE	$0.7\,g$		$0.9\,g$	
1.5%	MLE	$1.6987\,g$	0.5031	$2.8318\,g$	0.4327
	LR	$1.6174\,g$	0.6229	$2.3030\,g$	0.1604
	KDE	$1.8\,g$		$2.8\,g$	
2.5%	MLE	$2.4398\,g$	0.4664	$5.0177\,g$	0.3769
	LR	$2.7421\,g$	0.6229	$4.0640\,g$	0.1604
	KDE	$3.0\,g$		$5.1\,g$	

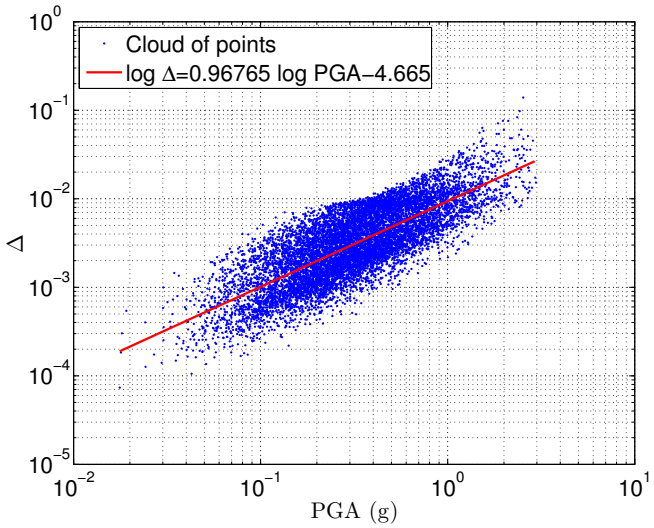

Figure 6. Paired data $\left\{(PGA_i, \Delta_i)\,, i = 1, \ldots, 10^4\right\}$ and linear regression in the logarithmic scale.

For the three considered drift thresholds, Figure 8 shows the lognormal (with two estimation approaches) and non-parametric (both MCS- and KDE-based) fragility curves when PGA is used as IM. One first observes a remarkable consistency between the curves obtained with the two proposed non-parametric approaches for all damage levels although the algorithms behind the methods are totally different. This validates the accuracy of the proposed approaches. For high values of PGA ($> 2\,g$), some noise is observed on the MCS curves due to the scarcity of observations in the corresponding intervals. This noise may be reduced by using additional observations in this range of PGA. Note, however, that the set of synthetic motions used in our analysis has statistical features characterizing the occurrence of actual earthquake motions (ground motions with large IMs have relatively low probabilities of occurrence). For the light damage level ($\delta_o = 0.7\%$), the parametric

Copyright © 2014 John Wiley & Sons, Ltd.
Prepared using eqeauth.cls

DOI: 10.1002/eqe

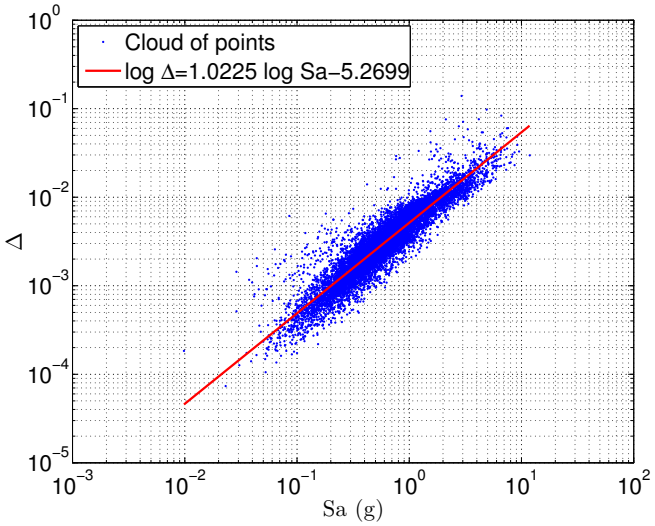

Figure 7. Paired data $\left\{\left(Sa_i, \Delta_i\right), i = 1, \ldots, 10^4\right\}$ and linear regression in the logarithmic scale.

curves are in fairly good agreement with the non-parametric curves. For the two higher damage levels, significant discrepancy is observed between the lognormal curves obtained with the different approaches as well as between the lognormal curves and the non-parametric ones. In particular, in the range of high PGA values, the lognormal curves tend to overestimate the failure probabilities.

Figure 9 shows the resulting fragility curves when Sa is used as IM. The non-pametric curves by MCS and KDE remain consistent independently of the damage level. The lognormal curves by MLE are close to the non-parametric curves except for the light damage level ($\delta_o = 0.7\%$). However, the lognormal curves by linear regression exhibit significant variations from the non-parametric curves for all damage levels. We note that linear regression estimation provides less accurate curves for Sa than for PGA, although the R^2 coefficient of the linear fit is higher for the former. This is due to the fact that the assumption of *normally distributed errors with constant variance*, which is inherent in Eq. (14), is not valid for Sa, as one observes in Figure 7. By considering a constant variance over the entire range of Sa values, the true variance in the regions of interest in fragility analysis is underestimated. Furthermore, under the assumption of a *unique linear model*, the median is overestimated at the lower drift limit and underestimated at the two larger drift limits. By providing a distinct pair of median and log-standard deviation estimates at each drift limit, the MLE approach outperforms linear regression.

The previous analysis shows that the two non-parametric approaches, namely MCS and KDE, yield consistent fragility curves for both IMs and for all considered damage levels. Using the non-parametric fragility curves as reference, the accuracy of the lognormal curves is found to depend strongly on the method for estimating the parameters of the underlying CDF, the considered IM and the drift threshold of interest. Note that different IMs have been recommended in literature [38, 42] for structures of different type, size and material. Accordingly, the accuracy of the lognormal fragility curves may depend on those factors as well. Possible dependency of the accuracy of the lognormal curves on the considered response quantity also needs to be investigated.

4.3. Estimation of statistical uncertainty by bootstrap resampling

Next, we use the bootstrap resampling technique (see Section 3.4) to investigate statistical characteristics of the fragility curves estimated with the proposed non-parametric approaches. In particular, we examine the stability of the estimates by comparing those with the bootstrap medians, and the uncertainty in the estimation by computing bootstrap confidence intervals. For the two considered IMs and the three damage levels of interest, Figure 10 shows the median MCS- and KDE-based fragility curves and the 95% confidence intervals obtained by bootstrap resampling

Copyright © 2014 John Wiley & Sons, Ltd.
Prepared using eqeauth.cls

DOI: 10.1002/eqe

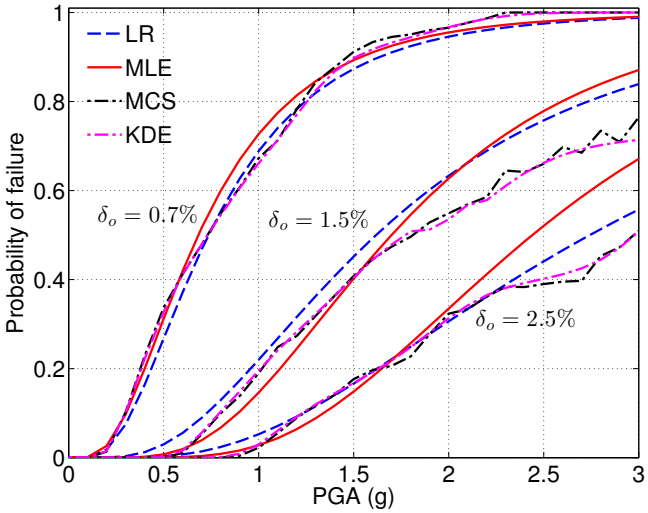

Figure 8. Fragility curves by parametric and non-parametric approaches using PGA as intensity measure.

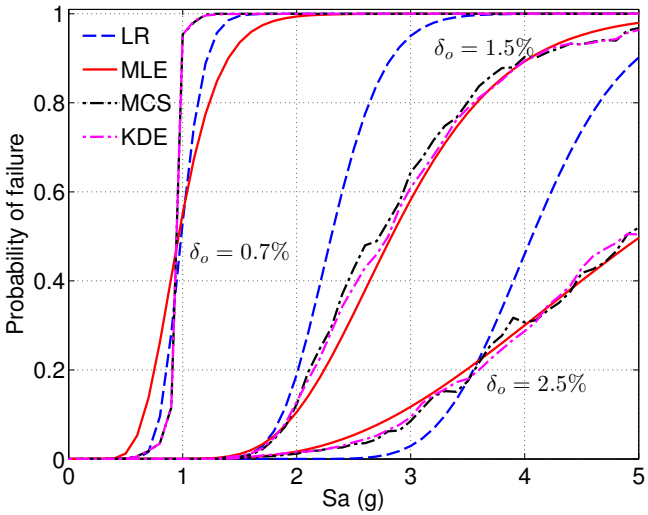

Figure 9. Fragility curves by parametric and non-parametric approaches using Sa as intensity measure.

with 100 replications. Figure 10 clearly shows that both the MCS-based and the KDE-based median fragility curves obtained with the bootstrap method do not differ from the curves estimated with the original set of observations. This shows the stability of the proposed approaches.

For a specified IM and drift limit, the confidence intervals of the MCS and KDE-based curves have similar widths. The interval widths tend to increase with increasing drift limit and increasing IM value. We note that for a certain drift limit and failure probability, the confidence intervals for the curves versus Sa tend to be narrower than for curves versus PGA. This is due to the higher correlation of structural responses with Sa.

5. CONCLUSIONS

Seismic fragility evaluation is one of the basic elements in the framework of performance-based earthquake engineering. At present, the classical lognormal approach is widely used to establish the seismic fragility curves. The approach consists in assigning the shape of a lognormal cumulative

Copyright © 2014 John Wiley & Sons, Ltd.
Prepared using eqeauth.cls

DOI: 10.1002/eqe

(a) Monte Carlo simulation approach (b) Kernel density estimation approach

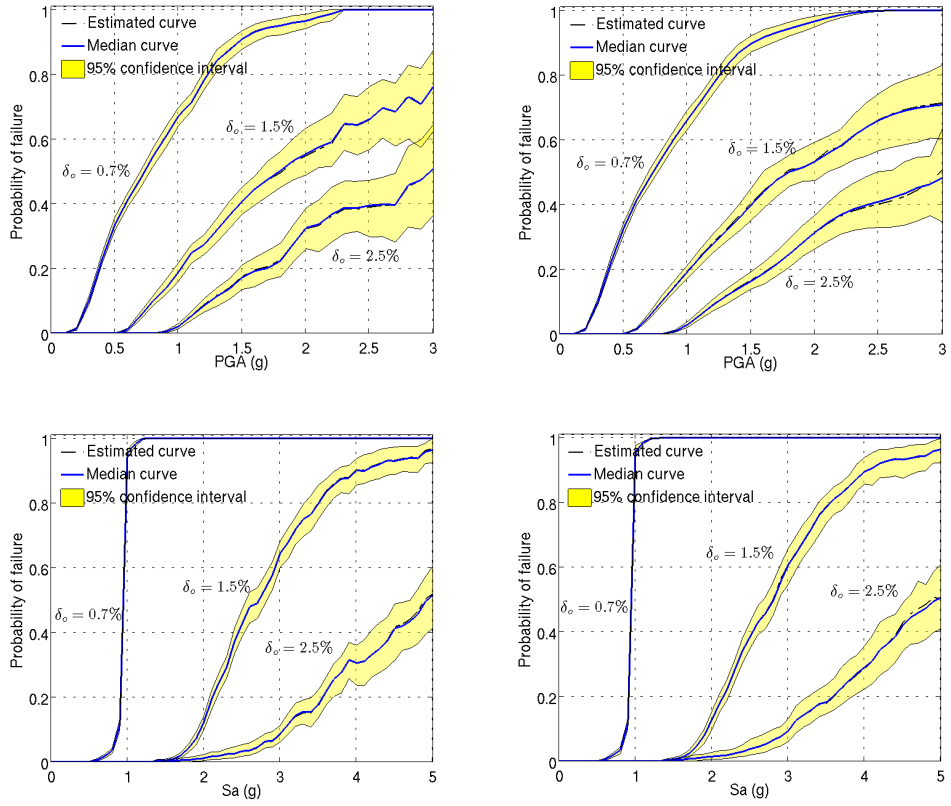

Figure 10. Estimated, mean bootstrap fragility curves and 95% confidence intervals by Monte Carlo simulation and kernel density estimation approaches. The mean curves and 95% confidence intervals are computed using bootstrap resampling technique with 100 replications.

distribution function to the fragility curves. However, the validity of this assumption remains an open question.

In this paper, we introduce two non-parametric approaches in order to examine the validity of the classical lognormal approach, namely the Monte Carlo simulation and the kernel density estimation. The former computes the crude Monte Carlo estimators for small subsets of ground motions with similar values of a selected intensity measure, while the latter estimates the conditional probability density function of the structural response given the ground motion intensity measures using the kernel density estimation technique. The proposed approaches can be used to compute fragility curves when the actual shape of these curves is not known as well as to validate or calibrate parametric fragility curves. Herein, the two non-parametric approaches are confronted to the classical lognormal approach on the example of a steel frame subject to synthetic ground motions.

In the case study, the fragility curves are established for three inter-storey drift-limit levels and two ground motion intensity measures, namely the peak ground acceleration (PGA) and the spectral acceleration (Sa). The non-parametric curves are consistent in all cases which proves the accuracy of the proposed techniques. Accordingly, these are used as reference to assess the accuracy of the lognormal curves. The parameters of the latter are estimated with two approaches, namely by maximum likelihood estimation and by assuming a linear probabilistic seismic demand model in the log-scale. It is shown that the accuracy of the lognormal curves is strongly dependent on the considered intensity measure and estimation method. Particularly large discrepancies between the

Copyright © 2014 John Wiley & Sons, Ltd.
Prepared using eqeauth.cls

DOI: 10.1002/eqe

non-parametric and the lognormal curves are observed under the assumption of a linear probabilistic seismic demand model in terms of Sa.

Use of the bootstrap resampling technique is proposed to estimate statistics of fragility curves. In the example application, this technique is employed to validate the stability of the non-parametric fragility curves and to compute confidence intervals of the estimated curves. For a certain damage level and failure probability, confidence intervals for the case of Sa, which is a structure-specific intensity measure, are narrower than for the case of PGA.

Further investigations are currently carried out in order to validate the current findings using real recorded ground motions and other type of structures.

Recently, fragility surfaces have emerged as an innovative way to represent the system's vulnerability [14] in which one calculates the failure probability conditional on two intensity measures of the earthquake motions. The computation of these surfaces is not straightforward and requires large computational effort. The present study opens new paths for establishing the fragility surfaces: Similarly to the case of fragility curves, one can use kernel density estimation to obtain assumption-free fragility surfaces that are consistent with the true ones obtained by Monte Carlo simulation.

The computational cost of the two proposed approaches remains significant since they are based on rather large Monte Carlo samples. In order to reduce this cost, alternative approaches may be envisaged. Polynomial chaos (PC) expansions [43, 44, 45, 46] appear as a promising tool. Based on a smaller sample set (typically a few hundreds of finite element runs), PC expansion provides a polynomial approximation that surrogates the structural response. The feasibility of post-processing PC expansions in order to compute fragility curves has been shown in [47, 48] in the case a linear structural behavior is assumed. The extension to nonlinear behavior is currently in progress.

REFERENCES

1. K A Porter. An overview of PEER's performance-based earthquake engineering methodology. In *Proc. 9th Int. Conf. on Applications of Stat. and Prob. in Civil Engineering (ICASP9), San Francisco*, pages 6–9, 2003.
2. R Campbell, G Hardy, and K Merz. Seismic Fragility Application Guide. Technical Report 1002988, EPRI, Palo Alto, 2002.
3. S Pei and J Van De Lindt. Methodology for earthquake-induced loss estimation: An application to woodframe buildings. *Structural Safety*, 31(1):31–42, 2009.
4. C A Cornell and H Krawinkler. Progress and challenges in seismic performance assessment. *PEER Center News*, 3(2):1–3, 2000.
5. J E Richardson, G Bagchi, and R J Brazee. The seismic safety margins research program of the U.S. Nuclear Regulatory Commission. *Nuc. Eng. Des.*, 59(1):15–25, 1980.
6. L Eads, E Miranda, H Krawinkler, and D G Lignos. An efficient method for estimating the collapse risk of structures in seismic regions. *Earthquake Engng Struct. Dyn.*, 42(1):25–41, 2013.
7. J Dukes, R DesRoches, and J E Padgett. Sensitivity Study of Design Parameters Used to Develop Bridge Specific Fragility Curves. In *Proc. 15th World Conf. Earthquake Eng.*, 2012.
8. E M Güneyisi and G Altay. Seismic fragility assessment of effectiveness of viscous dampers in R/C buildings under scenario earthquakes. *Structural Safety*, 30(5):461–480, 2008.
9. E Borgonovo, I Zentner, A Pellegri, S Tarantola, and E de Rocquigny. On the importance of uncertain factors in seismic fragility assessment. *Reliab. Eng. Sys. Safety*, 109(0):66–76, 2013.
10. T Rossetto and A Elnashai. A new analytical procedure for the derivation of displacement-based vulnerability curves for populations of RC structures. *Engineering Structures*, 27(3):397–409, 2005.
11. M Shinozuka, M Feng, J Lee, and T Naganuma. Statistical Analysis of Fragility Curves. *J. Eng. Mech.*, 126(12):1224–1231, 2000.
12. B R Ellingwood. Earthquake risk assessment of building structures. *Reliab. Eng. Sys. Safety*, 74(3):251–262, 2001.
13. I Zentner. Numerical computation of fragility curves for NPP equipment. *Nuc. Eng. Des*, 240:1614–1621, 2010.
14. D M Seyedi, P Gehl, J Douglas, L Davenne, N Mezher, and S Ghavamian. Development of seismic fragility surfaces for reinforced concrete buildings by means of nonlinear time-history analysis. *Earthquake Eng. Struct. Dyn.*, 39(1):91–108, 2010.
15. B Gencturk, A Elnashai, and J Song. Fragility Relationships for Populations of Woodframe Structures Based on Inelastic Response. *J. Earthq. Eng.*, 12:119–128, 2008.
16. B R Ellingwood and K Kinali. Quantifying and communicating uncertainty in seismic risk assessment. *Structural Safety*, 31(2):179–187, 2009.
17. S H Jeong, A M Mwafy, and A S Elnashai. Probabilistic seismic performance assessment of code-compliant multi-story RC buildings. *Engineering Structures*, 34:527–537, 2012.
18. S Banerjee and M Shinozuka. Mechanistic quantification of RC bridge damage states under earthquake through fragility analysis. *Prob. Eng. Mech.*, 23(1):12–22, 2008.

Copyright © 2014 John Wiley & Sons, Ltd.
Prepared using eqeauth.cls

DOI: 10.1002/eqe

19. E Choi, R DesRoches, and B Nielson. Seismic fragility of typical bridges in moderate seismic zones. *Eng. Struct.*, 26(2):187–199, 2004.
20. S Rezaeian and A Der Kiureghian. A stochastic ground motion model with separable temporal and spectral nonstationarities. *Earthquake Eng. Struct. Dyn.*, 37(13):1565–1584, 2008.
21. S Rezaeian and A Der Kiureghian. Simulation of synthetic ground motions for specified earthquake and site characteristics. *Earthquake Eng. Struct. Dyn.*, 39(10):1155–1180, 2010.
22. J Seo, L Duenas-Osorio, J I Craig, and B J Goodno. Metamodel-based regional vulnerability estimate of irregular steel moment-frame structures subjected to earthquake events. *Eng. Struct.*, 45:585–597, 2012.
23. J E Padgett and R DesRoches. Methodology for the development of analytical fragility curves for retrofitted bridges. *Earthquake Eng. Struct. Dyn.*, 37(8):1157–1174, 2008.
24. F Zareian and H Krawinkler. Assessment of probability of collapse and design for collapse safety. *Earthquake Eng. Struct. Dyn.*, 36(13):1901–1914, 2007.
25. D Vamvatsikos and C A Cornell. Incremental dynamic analysis. *Earthquake Eng. Struct. Dyn.*, 31(3):491–514, 2002.
26. M Mehdizadeh, K R Mackie, and B G Nielson. Scaling bias and record selection for fragility analysis. In *Proc. 15th World Conf. Earthquake Eng.*, 2012.
27. G P Cimellaro, A M Reinhorn, A D'Ambrisi, and M De Stefano. Fragility analysis and seismic record selection. *J. Struct. Eng.*, 137(3):379–390, 2009.
28. M Wand and M C Jones. *Kernel smoothing*. Chapman and Hall, 1995.
29. T Duong. *Bandwidth selectors for multivariate kernel density estimation*. PhD thesis, School of mathematics and Statistics, University of Western Australia, 2004.
30. T Duong and M L Hazelton. Cross-validation Bandwidth Matrices for Multivariate Kernel Density Estimation. *Scand. J. Stat.*, 32(3):485–506, 2005.
31. A D Frankel, C S Mueller, T P Barnhard, E V Leyendecker, R L Wesson, S C Harmsen, F W Klein, D M Perkins, N C Dickman, and S L Hanson. USGS national seismic hazard maps. *Earthquake spectra*, 16(1):1–19, 2000.
32. B Sudret and C V Mai. Calcul des courbes de fragilité par approches non-paramétriques. In *Proc. 21e Congrès Français de Mécanique (CFM21), Bordeaux*, 2013.
33. B Efron. Bootstrap methods: another look at the jackknife. *The annals of Statistics*, pages 1–26, 1979.
34. Pacific Earthquake Engineering Center and Research. OpenSees: The Open System for Earthquake Engineering Simulation, 2004.
35. G G Deierlein, A M Reinhorn, and M R Willford. Nonlinear structural analysis for seismic design. *NEHRP Seismic Design Technical Brief No*, 4, 2010.
36. Eurocode 1. *Actions on structures - Part 1-1: general actions - densities, self-weight, imposed loads for buildings*. 2004.
37. K Mackie and B Stojadinovic. Improving probabilistic seismic demand models through refined intensity measures. In *Proc. 13th World Conf. Earthquake Eng.* Int. Assoc. for Earthquake Eng. Japan, 2004.
38. J Padgett, B Nielson, and R DesRoches. Selection of optimal intensity measures in probabilistic seismic demand models of highway bridge portfolios. *Earthquake Eng. Struct. Dyn.*, 37(5):711–725, 2008.
39. Federal Emergency Management Agency, Washington, DC. *Commentary for the seismic rehabilitation of buildings*, 2000.
40. Eurocode 8. *Design of structures for earthquake resistance - Part 1: General rules, seismic actions and rules for buildings*, 1998.
41. T Duong. ks: Kernel Density Estimation and Kernel Discriminant Analysis for Multivariate Data in R. *J. Stat. Softw.*, 21(7):1–16, 2007.
42. S Jankovic and B Stojadinovic. Probabilistic performance based seismic demand model for R/C frame buildings. In *Proc. 13th World Conf. Earthquake Eng.*, 2004.
43. R Ghanem and P Spanos. *Stochastic Finite Elements : A Spectral Approach*. Courier Dover Publications, 2003.
44. M Berveiller, B Sudret, and M Lemaire. Stochastic finite elements: a non intrusive approach by regression. *Eur. J. Comput. Mech.*, 15(1-3):81–92, 2006.
45. G Blatman and B Sudret. An adaptive algorithm to build up sparse polynomial chaos expansions for stochastic finite element analysis. *Prob. Eng. Mech.*, 25(2):183–197, 2010.
46. G Blatman and B Sudret. Adaptive sparse polynomial chaos expansion based on Least Angle Regression. *J. Comput. Phys*, 230:2345–2367, 2011.
47. B Sudret, V Piquard, and C Guyonnet. Use of polynomial chaos expansions to establish fragility curves in seismic risk assessment. In G Lombaert G. De Roeck G. Degrande and G Müller, editors, *Proc. 8th Int. Conf. Struct. Dynamics (EURODYN 2011), Leuven, Belgium*, 2011.
48. B Sudret and C V Mai. Computing seismic fragility curves using polynomial chaos expansions. In G Deodatis, editor, *Proc. 11th Int. Conf. Struct. Safety and Reliability (ICOSSAR'2013), New York, USA*, 2013.

Copyright © 2014 John Wiley & Sons, Ltd.
Prepared using eqeauth.cls

DOI: 10.1002/eqe